PHYSICAL REVIEW C VOLUME 13, NUMBER 6 JUNE 1976

# $\Gamma_n/\Gamma_f$ for actinide nuclei using ($^3$He, $df$) and ($^3$He, $tf$) reactions*

A. Gavron,† H. C. Britt, E. Konecny,‡ J. Weber,§ and J. B. Wilhelmy
*Los Alamos Scientific Laboratory, University of California, Los Alamos, New Mexico 87545*

(Received 26 January 1976)

The fission probability was measured for a series of actinide nuclei as a function of the excitation enery using ($^3$He, $df$) and ($^3$He, $tf$) reactions. From these data, $\Gamma_n/\Gamma_f$ was determined from threshold up to ~12 MeV of excitation energy, and fitted by evaporation calculations which do not contain any arbitrary normalization factors. For heavier actinides, these fits are possible only if one assumes the fission process to proceed through a first saddle point which is *not* axially symmetric. These results and calculations also reproduce previously known empirical trends of average values of $\Gamma_n/\Gamma_f$, as a function of $A$ and $Z$.

[NUCLEAR REACTIONS, FISSION Measured fission probability in $^{230-233}$Pa, $^{231-232}$U, $^{233-239}$Np, $^{237-238}$Pu, $^{239-243}$Am, $^{241-244}$Cm. Determined barrier heights.]

## I. INTRODUCTION

During the past few years direct-reaction fission techniques have been used to obtain fission probability distributions $P_f = \langle \Gamma_f/(\Gamma_f + \Gamma_n + \Gamma_\gamma) \rangle$ on a wide variety of nuclei.[1,2] These distributions have been analyzed with various microscopic statistical models in an attempt to obtain systematic information for these nuclei on the heights and curvatures of the two peaks of the fission barrier ($E_A$, $\hbar\omega_A$, $E_B$, $\hbar\omega_B$). In the model used to fit the nonresonant fission probabilities for odd $A$ and odd-odd nuclei[1] it was found that an arbitrary normalization factor on $\Gamma_n/\Gamma_f$ had to be introduced in order to reproduce the correct magnitude of $P_f$, and in most cases the model still did not reproduce the shape of the $P_f$ distribution above the neutron binding energy.

The aim of the present series of experiments was to provide a systematic determination of $\Gamma_n/\Gamma_f$ from measurements of $P_f$ for an energy range of several MeV above the fission barrier and to interpret these results in terms of barrier heights and curvatures without employing any arbitrary normalization factors. This analysis is made possible by the use of microscopic level densities based on shell corrected single particle levels with the inclusion of the level density enhancement factors arising from the coupling of collective and intrinsic degrees of freedom in the nucleus.[3] We have found that the fission probability of the heavier actinides can be fitted *only* if it is assumed that the nucleus proceeds to fission through an axially asymmetric first saddle point. Thus these results provide evidence to support the theoretical predictions of axial asymmetry presented in Ref. 4. Our data agree qualitatively with the empirical trend of $\Gamma_n/\Gamma_f$ as a function of $Z$ and $A$ presented by Vandenbosch and Huizenga[5]; however, these empirical trends are averages over relatively large excitation energy bins, whereas our data provides detailed information on the excitation energy dependence of $\Gamma_n/\Gamma_f$.

($^3$He, $d$) and ($^3$He, $t$) reactions were chosen to form the various compound nuclei for two reasons: First, there are no light element contaminant peaks below excitation energies of ~11 MeV in the "singles" $d$ or $t$ spectra. Second, $^3$He breakup into $d+p$ was found to be unimportant in the excitation energy range considered. The fission probabilities of various compound nuclei formed by both ($^3$He, $d$) and ($^3$He, $t$) reactions (using different target nuclei) were compared and found to be approximately equal, thus providing some insight into the accuracy of the method. From this we estimate the overall systematic error in determination of $P_f$ to be less than 10%. Preliminary results of this work have been presented in Ref. 6.

## II. EXPERIMENTAL PROCEDURES AND DATA REDUCTION

### A. Experimental setup

The $^3$He beams were provided by the Los Alamos FN tandem Van de Graaff and the reactions performed at 25 MeV bombarding energy. Targets were prepared by vacuum evaporation on to ~50 $\mu$g/cm$^2$ carbon foils and were usually 80–200 $\mu$g/cm$^2$ thick. The experimental configuration is shown in Fig. 1. The light particles emitted by the nuclear reaction were detected in a $E$-$\Delta E$ counter telescope: The $\Delta E$ and $E$ detectors were 300 $\mu$m and 2 mm thick silicon surface barrier detectors,

respectively. The telescope was placed at 120° in order to eliminate the effect of carbon and oxygen contaminant peaks in the singles spectrum. Two fission detectors, $F1$ and $F2$, are placed at angles close to 0° and 90° relative to the recoil direction of the compound nucleus. The exact distance and angles in the laboratory are presented in Fig. 1. The fission detectors were 300 mm$^2$ surface barrier "heavy ion series" detectors.

The electronic instrumentation was similar to that described in Ref. 1. The use of a time-to-amplitude converter (TAC) to determine the fast coincidence requirement between a charged particle and a fission fragment enabled us to record simultaneously true and random coincidences; this facilitates subtraction of the random coincidence background, which was typically 2–4% of the total number of fission events.

The events (comprised of $E+\Delta E$, $\Delta E$, TAC, and fission detector pulse height signals) were recorded and analyzed on line by an SDS-930 computer. The computer program was able to identify the light particle by considering its position in the $(E+\Delta E)$, $\Delta E$ plane. It was thus possible to separate ($^3$He, $t$) events from the dominant ($^3$He, $d$) ones. The number of "single events" (i.e., particles not detected in coincidence with fission fragments) were scaled down by a factor of 10 or 100 in order to minimize the computer dead time.

The particle telescope was calibrated with the $^{208}$Pb($^3$He, $d$) reaction. Using this calibration and $Q$ values obtained from mass tables for the ($^3$He, $d$) and ($^3$He, $t$) reactions,[7] one obtains the compound nucleus excitation energy as a function of the $E+\Delta E$ pulse height for each target nucleus.

The solid angles subtended by the fission detectors were determined from a ratio of the counting rate at the distance used in the experiments to that for a distance of 10 cm from the source (where the solid angles can be determined accurately from the geometric dimensions).

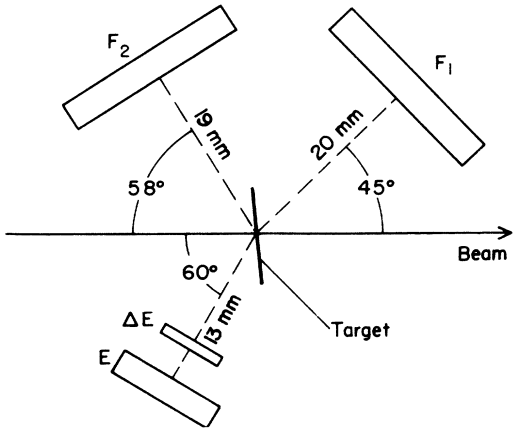


FIG. 1. Experimental setup.

### B. Data reduction

The fission probability $P_f$ is determined at each excitation energy from the ratio of the coincidence rate to the singles rate, using the expression

$$P_f(E_x)=\frac{2\pi}{\Omega}\frac{N_{\text{coin}}}{N_{\text{sing}}}(1+\tfrac{1}{3}\epsilon), \tag{1}$$

where $N_{\text{coin}}$ is the fission-particle coincidence rate in the 90° fission detector, $N_{\text{sing}}$ is the particle rate in the telescope, and $1+\epsilon$ is the ratio of the coincidence rates per unit solid angle in the 0° and 90° fission detectors, respectively. (This assumes a $1+\epsilon\cos^2\theta$ type angular distribution). Each of these rates, and hence $\epsilon$, are determined for each excitation energy (which is measured by the particle kinetic energy detected by the telescope). $\Omega$ is the solid angle subtended by the 90° fission detector. The fission angles are referred to the center of mass system for the recoiling nucleus. The fission probabilities were also corrected for various instrumental effects including:

(1) The dead time in the TAC (approximately 5 $\mu$sec per start pulse). At rates of 10 kHz, this amounts to 5% dead time. The rate of start pulses was recorded in each run, the dead time calculated, and the fission probability raised accordingly.

(2) Some of the targets used were found to be contaminated with tungsten. This does not effect the number of fission events, but increases the number of single events, thus decreasing the fission probability. The magnitude of the $W$ contaminant was determined by measuring $^3$He elastic scattering at 20 MeV beam energy at backward angles where the $W$ and actinide peaks could be resolved in energy. Appropriate corrections were made to the $P_f$ distributions. This method could detect contamination in the singles spectra of >2% and corrections to the data ranged from 0–15% except for $^{230}$Th, where a 30% correction was necessary. Details are presented in the Appendix.

## III. RESULTS

In the experimental fission probabilities the results were generally cut off above an excitation energy region of 11–12 MeV for one of the following reasons: (1) The ($^3$He, $d$) singles spectrum exhibits a large contaminant peak in the neighborhood of $E_x \sim 12$ MeV. (2) Above this excitation energy, the number of ($^3$He, $d$) and ($^3$He, $t$) events decreases rapidly because of the Coulomb barrier. (3) The triton spectrum is cut off because tritons with lower kinetic energy are stopped in the $\Delta E$ detector.

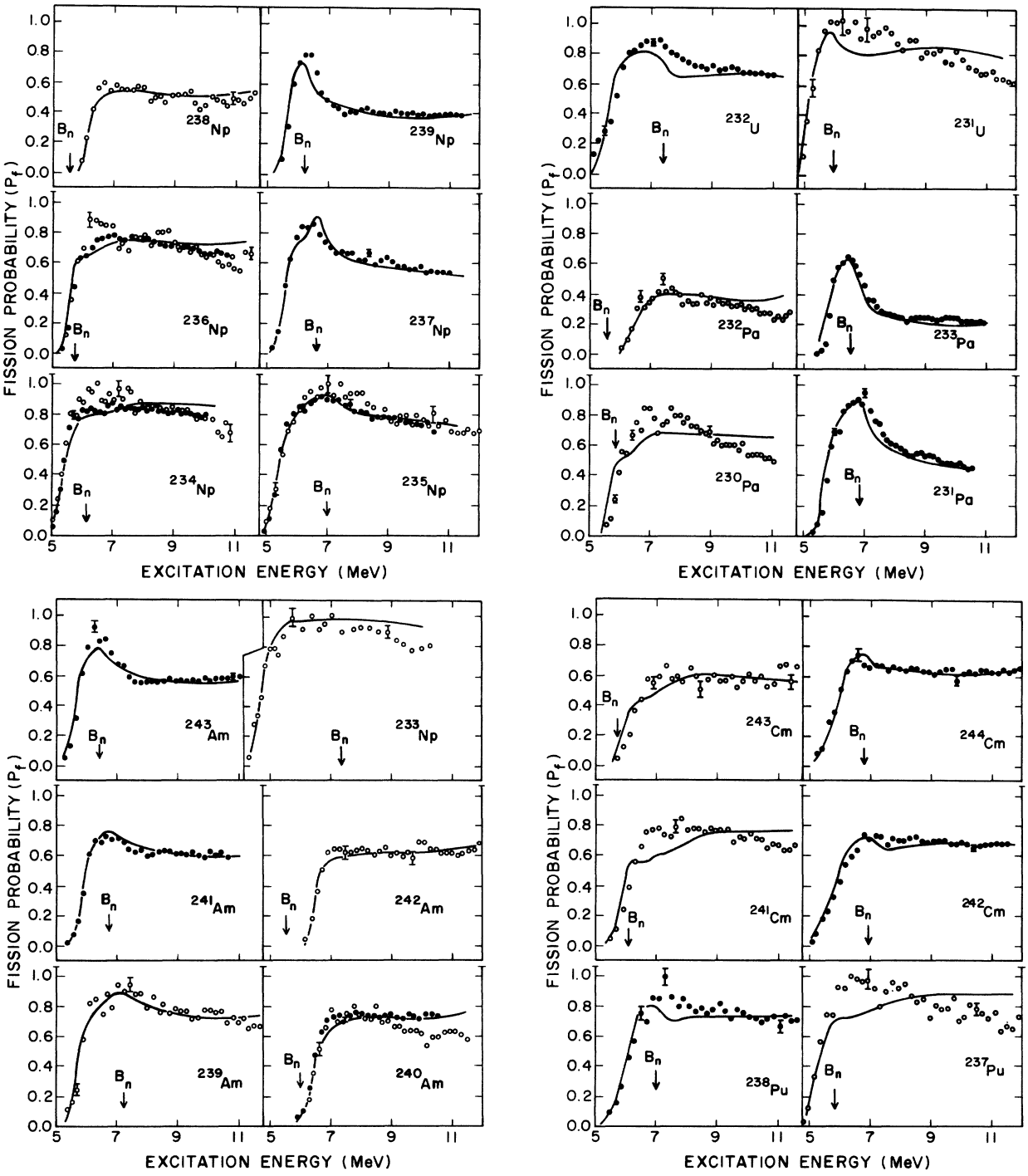


FIG. 2. Measured fission probabilities: open circles, from ($^3$He,$tf$) reactions; closed circles, from ($^3$He,$df$) reactions; full lines, model fits as discussed in the text.

The measured fission probabilities for the residual nuclei studied in this experiment are shown in Fig. 2. Typical systematic errors in the determination of absolute fission probabilities are less than 10%.

The fission probabilities for four compound nuclei ($^{234-236}$Np, $^{240}$Am) were determined using both ($^3$He, $d$) and the ($^3$He, $t$) reactions. This enables a

determination of the dependence of the fission probability on the reaction used to produce the compound nucleus. In general the maximum discrepancy between the two sets of data is 15%. However, somewhat above the fission barrier the difference is much smaller. This implies that there is no important contribution to the singles spectrum in the ($^3$He, $d$) results from the $^3$He "breakup" into a deuteron and proton in the energy range we have measured. If appreciable breakup occurred it would result in an increase in our measured singles spectrum and thus give an apparent lower fission probability. For the same compound nucleus the ($^3$He, $df$) fission probability would then appear smaller than that for the ($^3$He, $tf$) reaction, since breakup type reactions cannot contribute to the ($^3$He, $t$) singles spectra. The dip in the fission probability in $^{240}$Am from the ($^3$He, $t$) reaction at 10 MeV could possibly be due to an $^{18}$O contaminant peak in the singles spectra. Similar dips are noticeable in some of the other fission probabilities determined by the ($^3$He, $t$) reactions, at comparable excitation energies. Therefore, we may be systematically underestimating $P_f$ with the ($^3$He, $tf$) measurements in this energy region.

Our results can be compared with the general systematic trends presented by Vandenbosch and Huizenga.[5] These trends are presented in Fig. 3 together with our results for $\Gamma_n/\Gamma_f$ (obtained by assuming $P_f = \langle\Gamma_f\rangle/[\langle\Gamma_f\rangle + \langle\Gamma_n\rangle]$) (taken at excitation energies of 8 and 11 MeV corresponding approximately to 2 and 5 MeV, respectively, above the fission barrier). The results in Fig. 3 generally show that our measurements agree reasonably well with data previously obtained from $(n,f)$, $(\gamma,f)$, and spallation measurements. Near the region of $\beta$ stability our results show very little energy dependence for $\Gamma_n/\Gamma_f$. However, for very neutron-deficient nuclei a significant increase in $\Gamma_n/\Gamma_f$ with increasing $E_x$ is apparent.

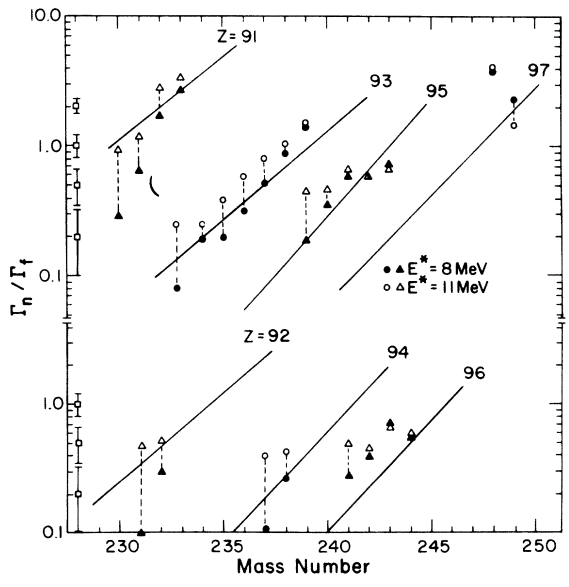


FIG. 3. $\Gamma_n/\Gamma_f$ values deduced from measured fission probabilities at 8 and 11 MeV excitation energy. Solid lines show the empirical trends of Vandenbosch and Huizenga (Ref. 5). Open squares at left indicate the uncertainty in $\Gamma_n/\Gamma_f$ due to a 10% uncertainty in $P_f$.

We have also compared calculated neutron-fission cross sections (obtained using our values for $\Gamma_n/\Gamma_f$ and reaction cross sections obtained from optical model calculations) to experimental cross sections. Good agreement was obtained. This is presented in detail in Ref. 8.

## IV. THEORETICAL ANALYSIS

The fission probabilities presented in the previous section were fitted using a modified version of a statistical model which was described in detail in Ref. 1. The model was modified so as to include the effects of collective enhancements to the intrinsic state densities. The intrinsic state densities were obtained from microscopic calculations using appropriate single particle levels. The most significant requirement for this analysis is that it is necessary to assume that the first saddle point is axially deformed in order to obtain adequate fits to higher mass ($A \gtrsim 235$) actinide nuclei.

In the following sections, we will present a brief review of the model presented in Ref. 1, explain how the collective enhancement effects are introduced, and discuss various aspects of the quality of the fits to the experimental data.

### A. Review of the statistical model

The statistical model considers the decay channels available to the excited compound nucleus. These are (1) $\gamma$ decay in the first well, (2) (above the neutron binding energy) neutron decay to the $A$-1 nucleus, and (3) transition over the first barrier to the second well. We assume the vibrational states in the second well to be completely damped into all the other compound states; in this case, a nucleus in the second well can either fission (over the second barrier) or return to the initial deformation over the first barrier. Denoting $N_A$ as the number of available transition states at the first barrier (at a specific excitation energy $E$, spin $J$, and parity $\Pi$) and, similarly, $N_B$ as the available states at the second barrier, the effective number of open channels to fission $N_f$ is

$$N_f = [N_A N_B/(N_A + N_B)]\, f\left(\frac{W_{II}}{D_{II}}\right), \qquad (2)$$

where $f(W_{II}/D_{II})$ is an additional factor which accounts for partial overlap between levels in the first and second wells (see Ref. 2), and is unity for excitations significantly above the two peaks of the fission barrier. Denoting as $N_n$ and $N_\gamma$ the number of channels open to neutron and $\gamma$ decay, respectively, $P_f$ is given by

$$P_f = \langle N_f/(N_f + N_n + N_\gamma)\rangle . \tag{3}$$

The average (again for fixed $E, J, \Pi$) is taken over the various compound states whose decay widths and level spacings fluctuate. Averaging over all possible angular momentum and parity values (as described in detail in Ref. 1) gives us the final values of $P_f(E_x)$ which can be compared directly to the experimental results. The number of open channels can be calculated using the appropriate level densities and transmission coefficients.[9] The intrinsic state densities were calculated from theoretical single particle level spectra[10] at the appropriate deformations using a microscopic state density code obtained from Moretto.[11] Level densities were obtained from the intrinsic state densities by incorporating collective enhancement effects as described below. For $E_x$ below 1 MeV the contribution of the discrete levels was calculated directly. Further details are presented in Ref. 1. Both the level densities and the discrete level spectrum of $^{240}$Pu were used throughout our calculations for all nuclei.

### B. Collective enhancement of level density

It has been noted that in previous fits to fission probability data[1] for actinide nuclei it was necessary to incorporate arbitrary normalization constants. Generally, it was necessary to decrease $\Gamma_n$ (or equivalently, increase $\Gamma_f$) by a sizeable factor in order to fit the data. Bjørnholm, Bohr, and Mottelson[3] have noted that deviations of a nucleus from spherical symmetry cause an increase in the level density due to the introduction of low lying rotational bands built on each intrinsic state. The incorporation of rotational enhancement factors for axially symmetric (deformed) nuclei has been investigated by Huizenga *et al.*[12] and by Dossing and Jensen.[13] They have found that by incorporating such enhancement factors in state densities calculated from realistic single particle levels, a reasonable agreement was obtained with measured neutron resonance spacings (no adjustable parameters were used in obtaining the agreement).

We denote $\omega(E)$ as the intrinsic state density at an excitation energy $E$. (This is obtained directly from single particle spectra without any adjustable parameters.) The level density $\rho(E,I)$ for a specific angular momentum $I$ in a spherical nucleus is[3]

$$\rho_{\rm sph}(E,I) = (2I+1)\exp[-I(I+1)/2\sigma^2(E)]\omega(E)/[(8\pi)^{1/2}\sigma^3(E)]. \tag{4}$$

The spin cutoff parameter $\sigma(E)$ (as a function of $E$) is obtained directly from the single particle spectrum using the same code.[11] Thus $\rho_{\rm sph}(E,I)$ is obtained without any adjustable parameters.

For a deformed, axially symmetric nucleus, rotational levels are important as long as the rotational energy is small compared to the temperature of the nucleus. Summing the level density over all the members of a rotational band built on each intrinsic state, one obtains[3]

$$\rho_{\rm ax}(E,I) = \{\omega(E)/[(8\pi)^{1/2}\sigma_{\|}(E)]\} \times \sum_{K=-I}^{I} \exp\left[-\frac{K^2}{2\sigma_{\|}^2(E)} - \frac{I(I+1)-K^2}{2\sigma_{\perp}^2(E)}\right]. \tag{5}$$

This is approximately equal to

$$\rho_{\rm ax}(E,I) \simeq (2I+1)\exp[-I(I+1)/2\sigma_{\perp}^2(E)] \times \omega(E)/[(8\pi)^{1/2}\sigma_{\|}(E)]. \tag{6}$$

$\sigma_{\|}$ is obtained from the single particle levels[11] and $\sigma_{\perp}$ is taken to be 5.45.[14] $\rho_{\rm ax}$ is enhanced relative to $\rho_{\rm sph}$ by a factor of $\sigma^3/\sigma_{\|} \simeq \sigma_{\|}^2(E)$ at each excitation energy $E$.

For a shape lacking any rotational symmetry, the level density $\rho_{\rm ns}(E,I)$ can be obtained by summing the intrinsic level density over all the rotational levels built on each intrinsic level. Denoting $E_r(K,I)$ as the rotational energy of a state having spin $I$ and an expectation value of $I_3$ (the component of the angular momentum along the intrinsic 3 axis) equal to $K$,

$$\rho_{\rm ns}(E,I) = \sum_K \omega[E - E_r(K,I)]. \tag{7}$$

$K$ runs over all the $2I+1$ possible projections. We obtain

$$\rho_{\rm ns}(E,I) \simeq (2I+1)\omega(E)\exp[-I(I+1)/2\bar{\sigma}^2(E)]. \tag{8}$$

$\bar{\sigma}$ is an average spin-cutoff parameter.

The approximation involved in this equation is good as long as $I < \bar{\sigma}$. Again, we note that $\rho_{\rm ns}$ is enhanced relative to $\rho_{\rm ax}$ by a factor of $\sim(8\pi)^{1/2}\sigma_{\|}$. Using levels of Ref. 10 to generate $\omega(E)$ and $\sigma(E)$,[11] the enhancement factor for a completely nonsymmetric first saddle point (relative to an axially symmetric one) ranges from 12 (at 1 MeV above the barrier) to 30 (6 MeV above the barrier). If

the saddle point possesses a point group rotational symmetry, the enhancement factor has to be divided by the order of the group.[3] Thus if the first barrier has a 180° rotation symmetry around a single axis, the enhancement factor is decreased by a factor of 2. If it has symmetry of rotation by 180° around three perpendicular axes [$D_2$ (ellipsoidal) symmetry], the enhancement factor is decreased by a factor of 4. At the second barrier, the level density is doubled because it is assumed to be reflection asymmetric.

The symmetry of the first barriers has of course a similar kind of effect on the discrete levels used in the first MeV: For an axially symmetric nucleus rotational bands are built on each one-quasiparticle state as described in Ref. 1. For a non-axially-symmetric nucleus, bands of an axially deformed rotor are built on each level,[15] and their number multiplied by a factor depending on the order of the point group symmetry. At the second barrier, levels of opposite parity (but equal energy) are added to the intrinsic levels because of the assumed reflection asymmetry.

### C. Procedures for fitting the data

We will now present a detailed explanation of how the assumption of lack of axial symmetry enables one to fit the experimental data.

Previous calculations[1] have shown that exclusion of the rotational enhancement factors results in fission probabilities which are too low. This can be seen in the attempted fit to $^{241}$Am in the upper part of Fig. 4 (dashed curve). However, including the rotational enhancement factors with the assumption that the first barrier is axially asymmetric results in an acceptable fit to the experimental data. In these fits the region near threshold determines the value of $E_A$, while the higher energy regions are sensitive to the value for $E_B$. The lower part of Fig. 4 shows the ratio of the number of open channels at the two barriers $N_A/N_B$. In the barrier region $N_A/N_B < 1$, $N_f \simeq N_A$ and the fission probability in the barrier region is determined by the height of the first barrier. High above the barrier, $N_A/N_B > 1$, $N_f \simeq N_B$ and it is the height of the second barrier which determines the fission probability. Summarizing, both $E_A$ and $E_B$ are determined for these cases when $P_f(E_x)$ is fitted over the entire range appropriate to first chance fission.

We now consider the case of point group symmetry at the first barrier: For ellipsoidal symmetry ($N=4$), $N_A$ is reduced relative to the non-symmetry case by a factor of 4. In order to retain the fit, $N_A$ or $N_B$ (or both) have to be increased; this is done by lowering $E_A$ or $E_B$ (or both). Considering Fig. 4 ($^{241}$Am), a good fit is obtained by lowering the outer barrier to 4 MeV, so that $N_A/N_B \ll 1$. In this case the fission probability is determined over the entire excitation energy range by $E_A$ and, therefore, only an upper limit can be set for $E_B$. As can be seen in Fig. 4, this does not cause significant deterioration in the fit. However, any further decrease in $N_A$ does not enable one to fit the experimental data: The curves marked

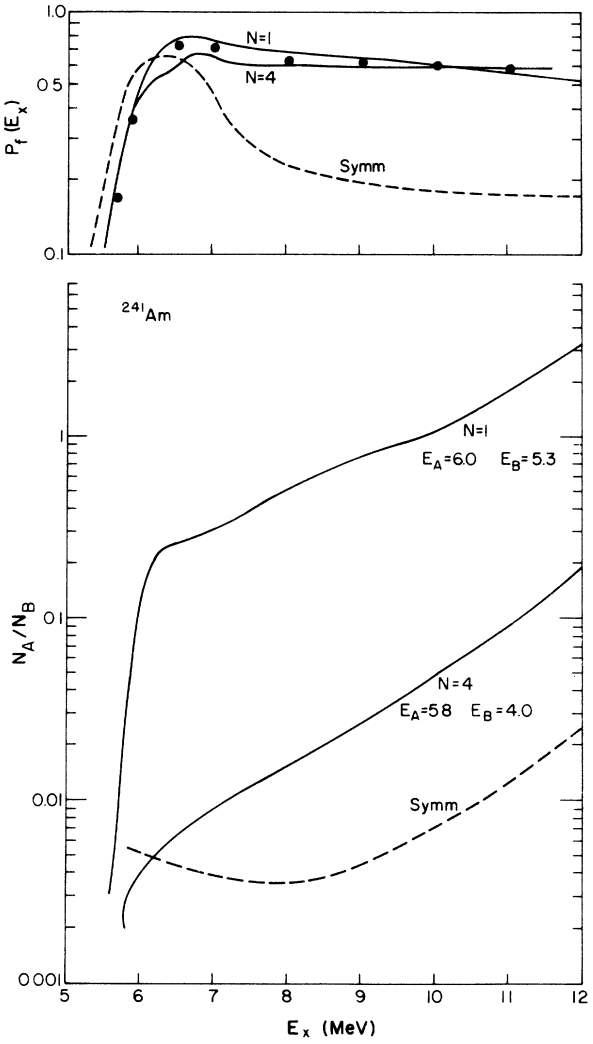


FIG. 4. The effect of different degrees of asymmetry at the first barrier on the model calculations in $^{241}$Am. $N=1$ implies no rotational symmetry, $N=4$ is $D_2$ (ellipsoidal) symmetry, and SYMM denotes axial symmetry at the first barrier. The upper part of the figure shows best fits to $P_f(E_x)$ for each use. The lower part shows the relative number of open channels at the two barriers. We see that at high excitation energies (for $N=1$) $N_B < N_A$, which enables us to fit $P_f$ by adjusting $E_B$. For the axially symmetric case, $N_A$ is too low to fit $P_f$, and no adjusting of $N_B$ can remedy this.

SYMM are attempted fits to the data assuming an axially symmetric first barrier. In all cases, $N_A$ is too small above the barrier to obtain a reasonable fit. No further lowering of $E_B$ (increasing $N_B$) can compensate for this, since $N_f \simeq N_A$. There are some nuclei which cannot be fitted when assuming axial asymmetry together with $D_2$ symmetry: the reduction in $N_A$ by a factor of 4 (relative to the no-symmetry case) produces a fission probability which is more than 10% lower than the experimental results. These nuclei are $^{238}$Pu, $^{242}$Am, and $^{242-244}$Cm.

### D. Results of calculations

Results of the statistical model calculations are presented in Fig. 2 along with the experimental results. The calculations employed level densities obtained from the single particle levels of Ref. 10.

We will later discuss the effects of using different sets of single particle levels. The calculated values of $P_f(E_x)$ presented in the figures were obtained when assuming the first saddle point to be devoid of any rotational point group symmetry.

The model calculations reproduce the experimental data quite accurately over the entire range of nuclei ($91 \leq Z \leq 96$, $230 \leq A \leq 244$) and excitation energies ($5 \leq E_x \leq 12$ MeV). There are, however, some systematic differences noticeable, especially in the even-odd nuclei. Immediately above the neutron binding energy, the calculated $P_f(E_x)$ levels off due to the neutron competition with fission. Such effects are not present in the experimental data.

The barrier parameters used in the calculations are summarized in Table I. We note that, generally, there is little difference between the parameters used when assuming no point group symmetry and the parameters used when assuming 180° rotational symmetry around a single axis at the first barrier ($N=2$). When assuming ellipsoidal ($D_2$) symmetry ($N=4$), the second barrier is often

TABLE I. Barrier parameters used in the analysis of the fission probabilities. $N$ is the order of the rotational point group assumed at the first barrier. SYMM shows results using an axially symmetric first barrier. These results were obtained using a harmonic oscillator potential (Ref. 10). The column labelled FY presents results obtained using the level density obtained from levels in Ref. 16 using a folded Yukawa potential. $\hbar\omega$ is the curvature of the higher of the two barriers. All units are MeV.

| | | $N=1$ | | | $N=2$ | | | $N=4$ | | | SYMM | | | FY($N=1$) | | |
|---|---|---|---|---|---|---|---|---|---|---|---|---|---|---|---|---|
| | | $E_A$ | $E_B$ | $\hbar\omega$ | $E_A$ | $E_B$ | $\hbar\omega$ | $E_A$ | $E_B$ | $\hbar\omega$ | $E_A$ | $E_B$ | $\hbar\omega$ | $E_A$ | $E_B$ | $\hbar\omega$ |
| Pa | 230 | 5.60 | 5.65 | 0.40 | 5.60 | 5.65 | 0.40 | 5.50 | 5.65 | 0.40 | 4.00[a] | 5.65 | 0.40 | 6.05 | 5.45 | 0.75 |
| | 231 | 5.95 | 5.70 | 0.80 | 5.85 | 5.60 | 0.70 | 5.70 | 5.60 | 0.60 | 3.80[a] | 5.80 | 0.50 | 6.10 | 5.80 | 0.80 |
| | 232 | 6.55 | 5.90 | 0.90 | 6.45 | 5.80 | 0.90 | 6.35 | 5.55 | 0.90 | 4.00[a] | 6.10 | 0.50 | 6.40 | 5.80 | 0.90 |
| | 233 | 5.30[a] | 6.00 | 1.10 | 5.70 | 6.00 | 1.10 | 5.30 | 5.95 | 0.70 | 4.00[a] | 5.90 | 0.55 | 6.01 | 6.00 | 0.70 |
| U | 231 | 5.20 | 5.40 | 0.65 | 5.00 | 5.40 | 0.60 | 4.80 | 5.40 | 0.55 | 3.80[a] | 5.50 | 0.55 | 5.20 | 5.40 | 0.90 |
| | 232 | 5.60 | 5.70 | 0.70 | 5.65 | 5.55 | 1.05 | 5.50 | 5.55 | 0.70 | 4.00[a] | 5.70 | 0.60 | 5.50 | 5.70 | 1.10 |
| Np | 233 | 5.35 | 4.95 | 1.15 | 5.25 | 4.95 | 1.15 | 5.10 | 4.95 | 1.15 | 3.80[a] | 5.30 | 1.15 | 5.35 | 4.95 | 1.05 |
| | 234 | 5.60 | 5.50 | 0.76 | 5.45 | 5.50 | 0.80 | 5.30 | 5.50 | 0.80 | 4.00[a] | 5.50 | 0.70 | 5.50 | 5.35 | 0.70 |
| | 235 | 5.80 | 5.30 | 0.85 | 5.70 | 5.30 | 0.85 | 5.60 | 5.10 | 0.80 | b | b | b | 5.80 | 5.40 | 0.80 |
| | 236 | 5.75 | 5.40 | 0.50 | 5.65 | 5.40 | 0.50 | 5.65 | 5.20 | 0.50 | 4.00[a] | 5.60 | 0.42 | 5.70 | 5.30 | 0.50 |
| | 237[c] | 5.70 | 5.30 | 0.50 | 5.65 | 5.10 | 0.50 | 5.60 | 4.80 | 0.47 | b | b | b | 5.80 | 5.40 | 0.50 |
| | 238[c] | 6.15 | 5.55 | 0.40 | 6.10 | 5.45 | 0.40 | 6.05 | 5.00 | 0.40 | b | b | b | 6.00 | 5.30 | 0.40 |
| | 239[c] | 5.70 | 5.20 | 0.40 | 5.65 | 5.00 | 0.38 | 5.60 | 4.60 | 0.33 | b | b | b | 5.80 | 5.20 | 0.45 |
| Pu | 237 | 5.60 | 5.10 | 0.80 | 5.45 | 5.10 | 0.80 | 5.35 | 5.00 | 0.70 | b | b | b | 5.60 | 5.50 | 0.90 |
| | 238[c] | 6.20 | 4.60 | 0.75 | 6.05 | 4.20[a] | 0.65 | b | b | b | b | b | b | 6.05 | 5.00 | 0.80 |
| Am | 239 | 5.30 | 5.50 | 0.63 | 5.75 | 5.40 | 0.63 | 5.70 | 5.30 | 0.63 | b | b | b | 6.05 | 5.30 | 0.75 |
| | 240[c] | 6.45 | 5.45 | 0.65 | 6.30 | 5.30 | 0.55 | 6.15 | 4.90[a] | 0.47 | b | b | b | 6.40 | 5.20 | 0.70 |
| | 241[c] | 6.00 | 5.10 | 0.55 | 5.95 | 4.80 | 0.55 | 5.80 | 4.00[a] | 0.48 | b | b | b | 6.20 | 4.80 | 0.70 |
| | 242[c] | 6.40 | 5.05 | 0.38 | 6.30 | 4.60[a] | 0.35 | b | b | b | b | b | b | 6.20 | 5.10 | 0.30 |
| | 243[c] | 5.75 | 4.95 | 0.50 | 5.70 | 4.60 | 0.50 | 5.55 | 4.00[a] | 0.32 | b | b | b | 5.85 | 4.95 | 0.50 |
| Cm | 241[c] | 6.00 | 5.65 | 0.70 | 5.90 | 5.55 | 0.70 | 5.90 | 5.20[a] | 0.70 | b | b | b | 6.20 | 5.50 | 0.55 |
| | 242[c] | 6.25 | 4.60 | 1.10 | 5.95 | 4.20[a] | 0.80 | b | b | b | b | b | b | 6.10 | 4.95 | 1.00 |
| | 243[c] | 5.95 | 5.50 | 0.60 | 5.75 | 5.20[a] | 0.45 | b | b | b | b | b | b | 6.40 | 4.90 | 0.80 |
| | 244[c] | 6.20 | 4.60 | 0.90 | 6.03 | 4.00[a] | 0.90 | b | b | b | b | b | b | 6.10 | 4.50 | 0.95 |

[a] These values should be considered an upper limit.
[b] Cannot be analyzed using these assumptions.
[c] Second barrier strongly dependent on collective enhancement at first barrier.

markedly lower and, in some cases, no fit is possible at all.

## V. DISCUSSION

The two main conclusions we have drawn which should now be discussed in terms of the errors involved are: (1) The first barrier of the heavier actinide nuclei is axially deformed; (2) both the first and the second barrier heights ($E_A$ and $E_B$) are determined by the high energy fission probability data for a significant number of nuclei.

Since the barrier parameters determined from fits to experimental fission probabilities are model dependent, it is now appropriate that we should consider how they relate to previously calculated properties of the fission barrier and how various assumptions and calculations used can effect our results.

It is important to stress that these experiments sample the saddle point of the level density in the multicoordinate space rather than the potential energy surface saddle point. Thus, an axially symmetric potential energy surface which is soft towards $\gamma$ vibrations can give rise to fission through an axially deformed level density saddle point if the symmetry breaking enhances the level density enough to offset its decrease due to a decrease of excitation energy.

Our conclusion that the first barrier is axially deformed is compatible with various theoretical calculations[4] which indicate that the first barrier would be decreased by ~1 MeV for the heavier actinides by axially deforming the nuclear shape.

### A. Systematic uncertainties

#### *1. Level densities*

Our conclusions regarding the degree of symmetry of the transition state depend on the accuracy of the level densities and neutron transmission coefficients involved. To check these effects we have used different level densities and different transmission coefficients. The effect of using different intrinsic single particle levels to generate the level densities can be seen in Table I. Barrier parameters obtained using single particle levels of Bosterli *et al.*[16] at the first minimum and at the two saddle points are compared to parameters obtained using the Nilsson type single particle levels[10] at the first minimum and at the first barrier. These two sets of single particle levels used to generate the compound level density are calculated using different physical assumptions. The single particle levels of Bolsterli *et al.*[16] were calculated using axially symmetric shapes, whereas the Nilsson single particle levels were calculated for an axially deformed first barrier. Despite these physical differences, one set of level densities never differs from the other by more than a factor of 2, over the first 10 MeV range of excitation energy. This is true both for the ground state deformation and that of the maxima and is due to the fact that the shell and pairing phenomena have opposite effects on the level density at low ($\lesssim$10 MeV) excitation energies. If the single particle level spacing is large ("shell"), the pairing gap $\Delta$ will be small and so will the temperature $T$. Since $d(\ln\rho)/dE = 1/T$ ($\rho$-compound level density), $\rho$ will increase faster, offsetting the effect of the low single particle density. We can therefore, conclude that the error in $\rho$ involved in the intrinsic level density at the barriers and minima is at most a factor of ~2. Our conclusion of the existence of axial asymmetry at the first barrier is based on the necessity for an enhancement factor which increases the level density by at least a factor of 10 in order to provide a consistent fit to the data for all the nuclei we analyzed. Such a factor cannot be due to systematic errors in the level density and we thus conclude that the compound nucleus fissions through an axially deformed first barrier.

#### *2. Enhancement factors*

The determination of the order of point group symmetry of the first barrier is more questionable. If we assume the first barrier to have 180° rotational symmetry around a single axis, the enhancement factor is reduced twofold. The $P_f(E_x)$ results can then be fitted with slightly modified barrier parameters (see Table I). This is not so for $D_2$ symmetry (180° rotational symmetry around three perpendicular axes). Some nuclei cannot be fitted at all when the enhancement factor is divided by 4. We do not, however, think that this is conclusive evidence of the lack of $D_2$ symmetry at the first saddle point due to possible errors in the level density. Discrepancies of factors of 2 in calculated level densities (and occasionally larger) were also observed by Huizenga *et al.*,[12] who compared calculated level densities to measured neutron resonance spacings at the neutron binding energy of a large number of deformed nuclei. Vibrational enhancements to the level density have not been included in our analysis. Crude estimates of frequencies involved indicate that these enhancement effects could be a factor of 2–4. Therefore, it is possible that the first barrier has $D_2$ rotational symmetry but the level density is approximately equal to that of a barrier lacking any rotational symmetry ($N=1$ in Table I) due to the increase of level density caused by vibrational enhancements.

Throughout the analysis we have assumed the

second barrier to be axially symmetric and mass asymmetric. This results in a factor of 2 enhancement to the level density at the second barrier. Additional enhancement factors could be incorporated at the second barrier. These would modify the height of the second barrier determined by fitting the data and large changes could be expected for cases where $E_B \ll E_A$. Therefore, in many cases the determination of the height of the second barrier is model dependent. This is particularly true for those cases which show large changes in $E_B$ when fits are performed using different point group symmetries at the first barrier. Similarly, for some light nuclei where $E_A < E_B$, values of $E_A$ are also model dependent. In addition, if large enhancements were present at the second barrier then there are many cases where the first and second barriers could be interchanged in the present analysis.

### B. Uncertainties in barrier parameters

We now summarize the various errors which contribute to the total error in the determined barrier heights. There are two major factors in the total error: (1) errors in the data used as input to the model; (2) errors due to various inadequacies and lack of complete knowledge of the symmetries and enhancement factors in the model itself.

The first category contains errors in the level densities and in the neutron transmission coefficients used to calculate the neutron decay width. We have already pointed out that the error in level densities in the energy range considered is at most of the order of a factor of 2. Comparing the first and last columns of Table I shows the effect of using level densities generated from different single particle levels: average differences are of the order of 0.1–0.2 MeV, although in certain cases there are differences of 0.4 MeV.

Selection of a set of neutron transmission coefficients also has a significant effect on the barrier heights determined by the model fits. In our calculations we have used the transmission coefficients produced by optical model calculations with the parameters of Rosen *et al.*[17] Use of other sets of transmission coefficients generally resulted in a higher calculated probability; in order to refit the data, the barriers had to be raised. As an extreme case, the Blatt and Weisskopf[18] transmission coefficients were used to reanalyze $^{237}$Np and $^{241}$Cm. Using the barrier parameters of Table I, the average fission probability was increased by 20% in $^{237}$Np and by 8% in $^{241}$Cm. In order to refit the data, the second barrier had to be raised by 0.2 MeV in both cases.

A similar analysis shows the effect of a 10% error in the measured fission probability on the determined barrier heights assuming $E_A > E_B$: The first barrier is generally effected to a very small extent ($\lesssim$0.1 MeV). The second barrier (which determines the overall normalization) generally can be changed by 0.1–0.3 MeV by this error. For $E_A < E_B$ generally only an upper limit on $E_A$ can be set which is not very sensitive to the overall normalization.

We now discuss the model dependency of the barrier heights. Considering Table I, we see the effect of the point group symmetry at the first barrier ($N$ the order of the point group) on the barriers. The differences between the barrier heights using different point group symmetries are of the order of 0.2 MeV although there are much bigger differences in certain cases. In these cases, the lower of the two barriers is most sensitive to the degree of collective enhancement at the first barrier and the results should be regarded with extreme caution. If additional symmetry breaking occurs at the second barrier, $E_B$ would have to be raised accordingly to compensate for the enhancement involved.

Significantly different barriers resulting from different symmetry assumptions exist in the protactinium-uranium region: In this region the data can be analyzed when assuming an axially symmetric first barrier. This can be done by lowering the first barrier by 1.5–2.0 MeV without significantly changing the second barrier.

Two additional model dependent factors should be mentioned, although we have no quantitative estimate of their effect. First, the collective enhancement factors are essentially due to states which are at high energies in nondeformed nuclei that come down to low energies at some finite deformation. This implies that at higher excitation energies these states will be missing and the enhancement factor may consequently decrease with increasing $E_x$. It is not obvious where the enhancement factor starts decreasing. (See Ref. 3 and the discussion following it.) Second, the dynamic saddle point at high excitation energies could be completely different from the saddle point at low energies which is probably close to the potential energy surface saddle points. A possible example of such an effect could be the increase in symmetric fission at higher excitation energies.

No attempt has been made in this work to provide a detailed fit to the shape of the fission probability curve in the barrier region. The height of the second barrier was generally determined from the fission probability above the barrier. The height and curvature of the first barrier were determined by the fit to the barrier region; however, the curvature results should not be taken literally

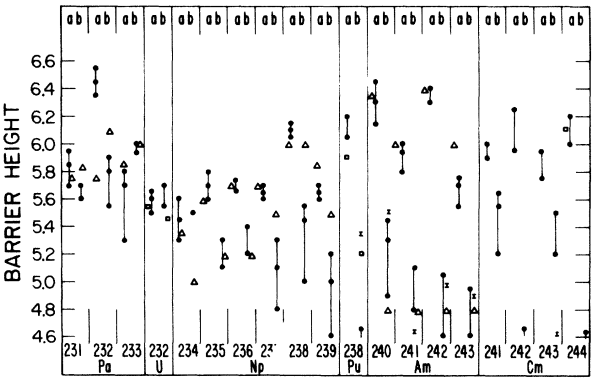


FIG. 5. Comparison of barrier heights obtained here (full circles, the lower points corresponding to the higher degree of point group symmetry at the first barrier) to those obtained in Ref. 1 (triangles), Ref. 2 (squares), and Ref. 19 ($I$ symbol). The left side of each column is the first barrier and the right side, the second barrier.

since the quality of the fits in this region often leaves much to be desired. This is probably due to the nonparabolic shape of the actual barrier.[16] (Alternatively we can say that $\hbar\omega$ changes as a function of $E_x$, an effect which is not included in our model which assumes the barrier to have a parabolic shape.)

As a final check on the degree of model dependence, Fig. 5 presents a comparison of barriers determined here, to those determined by resonance fitting[2] and by isomer excitation function data,[19] together with barriers obtained previously when arbitrary normalization factors were included.[1] The agreement is generally good although there are a few cases in which there are discrepancies of the order of 0.5 MeV.

## VI. SUMMARY

We summarize our results as follows:

(1) ($^3$He, $d$) and ($^3$He, $t$) reactions can be used to obtain fission probabilities (and hence $\Gamma_n/\Gamma_f$) up to excitation energies of ~12 MeV. We estimate the overall error in $P_f$ to be on average less than 10%.

(2) The statistical model we have used can reproduce the experimental data with reasonable agreement both in the overall magnitude and in the general trend.

(3) The assumption that the first barrier is axially deformed is essential to the fit for the heavier actinides and consistent with results for lighter actinides.

(4) For many nuclei both the first and second barrier heights ($E_A$ and $E_B$) are determined but in some cases the height of the lower barrier is dependent on the symmetries assumed at that point. The uncertainties involved are of the order of ±0.2 MeV for the highest barrier and the barrier heights determined here generally agree with previously published values.[1,2,19]

## ACKNOWLEDGMENTS

The authors would like to thank Professor A. Bohr for stimulating discussions. We would also like to thank J. R. Nix, S. E. Larsson, P. Möller, S. G. Nilsson, and A. Kerman for their comments on various aspects of this work. We are grateful to S. E. Larsson, P. Möller, and J. R. Nix for making available their codes for calculating single particle level spectra and to L. G. Moretto for the use of his code for calculating compound level densities.

## APPENDIX: CORRECTION TO "SINGLES" SPECTRUM FOR THE CONTRIBUTION OF TUNGSTEN CONTAMINANT

We denote $N(E)$ the "singles" energy spectrum at an excitation energy of $E$. (The same treatment applies to deuterons and tritons.) $N(E)$ is the sum of the actinide "singles" $U(E)$ and the tungsten singles $W(E)$:

$$N(E) = U(E) + W(E) = U(E)[1 + W(E)/U(E)]. \quad \text{(A1)}$$

$W(E)/U(E)$ is determined as follows: Denoting the $^3$He elastic intensity at a bombarding energy $E_0$, $U_{el}(E_0)$ (for the actinide), and $W_{el}(E_0)$ (for tungsten), the correction factor $1/f(E)$ is determined by

$$f(E) = 1 + W(E)/U(E)$$
$$= 1 + \left\{\left[\frac{W(E)}{W_{el}(25)}\right] \Big/ \left[\frac{U(E)}{U_{el}(25)}\right]\right\} \frac{W_{el}(25)}{E_{el}(25)}, \quad \text{(A2)}$$

where $W(E)/W_{el}(25)$ and $U(E)/U_{el}(25)$ are determined at 25 MeV for a tungsten and actinide target. $W_{el}(25)/U_{el}(25)$ is determined by

$$\frac{W_{el}(25)}{U_{el}(25)} = \frac{W_{el}(20)}{U_{el}(20)} \frac{W_{el}(25)}{W_{el}(20)} \frac{U_{el}(20)}{U_{el}(25)}. \quad \text{(A3)}$$

The elastic peaks are well separated at 20 MeV and the ratios $W_{el}(25)/W_{el}(20)$ and $U_{el}(20)/U_{el}(25)$ are determined by using tungsten and actinide targets, respectively, and normalizing to a unit current integrator value.

*Work supported by the U.S. Energy Research and Development Administration.

†On leave of absence from the Weizmann Institute of Science, Rehovot, Israel.

‡Current address: Drägewerk, Postfach 1339, 24 Lübeck, West Germany.

§Current address: Sektion Physik, Universität München, München, West Germany.

[1]B. B. Back, H. C. Britt, O. Hansen, B. Leroux, and J. D. Garrett, Phys. Rev. C 10, 1948 (1974).

[2]B. B. Back, O. Hansen, H. C. Britt, and J. D. Garrett, Phys. Rev. C 9, 1924 (1974).

[3]S. Bjørnholm, A. Bohr, and B. R. Mottelson, in *Proceedings of the Third International Atomic Energy Symposium on the Physics and Chemistry of Fission, Rochester, 1973* (International Atomic Energy Agency, Vienna, 1974), Vol. I, p. 367.

[4]S. E. Larsson and G. Leander, in *Proceedings of the Third International Atomic Energy Symposium on Physics and Chemistry of Fission, Rochester, 1973* (see Ref. 3), Vol. I, p. 177; U. Götz, H. C. Pauli, and K. Junker, Phys. Lett. 39B, 436 (1972).

[5]R. Vandenbosch and J. R. Huizenga, *Nuclear Fission* (Academic, New York, 1973), p. 227.

[6]A. Gavron, H. C. Britt, E. Konecny, J. Weber, and J. B. Wilhelmy, Phys. Rev. Lett. 34, 827 (1975).

[7]A. H. Wapstra and N. B. Gove, Nucl. Data A9, 5 (1971).

[8]J. B. Wilhelmy, H. C. Britt, A. Gavron, E. Konecny, and J. Weber, in *Proceedings of the Conference on Nuclear Cross Sections and Technology, Washington, D. C., March 3–7, 1975* (National Bureau of Standards Special Publication No. 425, 1975), Vol. I, p. 218.

[9]H. C. Britt, S. C. Burnett, B. H. Erkkila, J. E. Lynn, and W. E. Stein, Phys. Rev. C 4, 1444 (1971).

[10]S. E. Larsson (private communication); P. Möller (private communication).

[11]L. G. Moretto (private communication). The authors would like to thank Dr. Moretto for providing them with the level density calculation code.

[12]J. R. Huizenga, A. N. Behkami, R. W. Atcher, J. S. Sventek, H. C. Britt, and H. Freiesleben, Nucl. Phys. A223, 589 (1974).

[13]T. Dossing and A. S. Jensen, Nucl. Phys. A222, 493 (1974).

[14]A. Gilbert and A. G. W. Cameron, Can. J. Phys. 43, 1446 (1965).

[15]M. A. Preston, *Physics of the Nucleus* (Addison-Wesley, Reading, Massachusetts, 1962), p. 243.

[16]M. Bolsterli, E. O. Fiset, J. R. Nix, and J. L. Norton, Phys. Rev. C 5, 1050 (1972); J. R. Nix (private communication).

[17]L. Rosen, J. G. Beery, A. S. Goldhaber, and E. H. Auerbach, Ann. Phys. (N.Y.) 34, 96 (1965).

[18]J. M. Blatt and V. F. Weisskopf, *Theoretical Nuclear Physics* (Wiley, New York, 1952), pp. 342–365.

[19]H. C. Britt, M. Bolsterli, J. R. Nix, and J. L. Norton, Phys. Rev. C 7, 801 (1973).